Robust Time-Frequency Analysis of Multiple FM Signals with Burst Missing Samples

Shuimei Zhang, Yimin D. Zhang, *Fellow, IEEE*

***Abstract*—In this letter, we consider sparsity-based time-frequency representation (TFR) of frequency modulated (FM) signals in the presence of burst missing samples. In the proposed method, three key procedures are used to mitigate the effect of missing samples. First, each slice in the instantaneous autocorrelation function (IAF) corresponding to the time or lag domain is converted to a Hankel matrix, and whose missing entries are recovered via the atomic norm-based approach. Second, a signal-adaptive time-frequency kernel is used to mitigate the undesired cross-terms and the residual artifacts due to missing samples. Third, we apply a rank deduction technique on the obtained IAF to provide reliable TFR reconstruction results.**

***Index Terms*—Time-frequency analysis, burst missing samples, atomic norm, sparse reconstruction, nonstationary signal.**

I. Introduction

FREQUENCY modulated (FM) signals with time-varying instantaneous frequency (IF) are an important class of nonstationary signals, which find broad applications such as in radio astronomy, vibration acoustic, and communication [1]–[6]. Time-frequency representation (TFR) plays an important role in nonstationary signal analysis. In practice, missing data samples may occur in the received signal due to, e.g., impulsive noise removal, or intentional undersampling. Such missing samples prohibit providing accurate IF estimation based on conventional time-frequency (TF) analysis methods.

In recent years, several methods have been developed to enable robust TFR in the presence of random missing samples [7], [8]. TF kernels are used to mitigate the effects of artifacts due to missing samples while suppressing cross-terms, and compressive sensing-based methods are exploited to utilize the sparsity in the TF domain [7]. Compared to random missing samples, a more realistic and more challenging problem is the existence of burst missing data samples [9]–[11], which may arise from propagation fading and measurement obstructions.

A missing data iterative adaptive (MIAA) approach [12] was developed for spectrum analysis of stationary signals with arbitrary missing patterns. However, this method is not suitable to directly deal with nonstationary signals. Recognizing the behavior of missing samples to be similar to their local neighborhoods, an interpolation method based on empirical mode decomposition was developed in [13], but it becomes inefficient when few samples are available around the missing bursts. A data-dependent TF kernel was developed in [14] based on the minimization of the Gini's index. By utilizing the stationarity of the instantaneous auto-correlation function (IAF) with respect to the lag, an iterative sparse reconstruction approach is developed to fill in IAF missing entries [11]. However, both methods [14] and [11] do not perform well for multi-component signals with distinct strengths because the TFR of the weak signal component may be obscured by the residual artifacts of the stronger ones. An adaptive local filtering-based directional TF distribution method was proposed in [10] to handle multi-component signals with distinct magnitudes in the presence of burst missing samples. However, the success of this method replies on the performance of kerneled TFR.

In this letter, we propose a new approach that robustly reconstruct the TFR of multiple FM signals with distinct magnitudes in the presence of burst missing samples. Based on the fact that artifacts resulting from missing samples can be mitigated by interpolating the associated missing entries in the IAF while suppressing the cross-terms using TF kernels, the proposed method improves the IAF such that it is close to the adaptively kerneled IAF obtained from the full data without missing samples. Toward this end, the proposed method first recovers missing entries through interpolation using the atomic norm approach, and then applies the adaptive optimal kernel (AOK) [15] to the interpolated IAF to mitigate the effect of cross-terms and further reduces the residual effect of missing samples. In addition, we utilize the rank deduction technique on the interpolated and kerneled IAF and apply sparse TFR reconstruction technique to further improve the TFR.

Notations: Lower-case (upper-case) bold characters are used to denote vectors (matrices). $(\cdot)^*$, $(\cdot)^{\mathrm{T}}$ and $(\cdot)^{\mathrm{H}}$ denote the complex conjugation, transpose and the Hermitian transpose, respectively. $\mathcal{F}_x(\cdot)$ and $\mathcal{F}_x^{-1}(\cdot)$ represent the discrete Fourier transform (DFT) and inverse DFT (IDFT) with respect to x, respectively. $\mathrm{diag}(\cdot)$ denotes a vector consisting of the diagonal elements of a matrix. $\boldsymbol{Y} = \mathcal{H}(\boldsymbol{x}, p)$ converts vector $\boldsymbol{x}$ to Hankel matrix $\boldsymbol{Y}$ with pencil parameter p, whereas $\boldsymbol{x} = \hbar(\boldsymbol{Y})$ defines the inverse operation of Hankel matrix conversion. $\lceil\cdot\rceil$ denotes the ceiling function. $\mathcal{T}(\boldsymbol{x})$ denotes a Hermitian Toeplitz matrix with $\boldsymbol{x}$ as its first column.

II. Signal Model and Time-Frequency Representations

A. Signal Model

Consider a discrete-time signal, $x(t), t = 1, \cdots, T$, which consists of a single or multiple FM components. Denote $r(t)$ as its observation data with L missing data bursts. The bursts of missing samples are randomly and uniformly distributed over time and do not overlap with each other.

The received signal $r(t)$ can be taken as the product of the original signal $x(t)$ and an "observation mask", $R(t)$, i.e.,

$$r(t) = x(t) \cdot R(t). \tag{1}$$

This work is supported in part by the National Science Foundation (NSF) under grant AST-1547420.

The authors are with the Department of Electrical and Computer Engineering, Temple University, Philadelphia, PA 19122.

Here, $R(t)$ is a binary sequence, whose elements are 1 for the observed samples and 0 for the missing samples.

B. Instantaneous Auto-correlation Function

The IAF of $x(t)$ is defined as

$$R_{xx}(t,\tau) = x(t+\tau)x^*(t-\tau), \tag{2}$$

where τ is the time lag. Recalling (1), the IAF of $r(t)$ is expressed as

$$R_{rr}(t,\tau) = R_{xx}(t,\tau)R_{RR}(t,\tau), \tag{3}$$

where $R_{RR}(t,\tau)$ is the IAF of the observation mask $R(t)$. Each burst of missing data samples results in a missing IAF strip, which causes a convolving sinc function applied to the TF domain. Therefore, sinc-like artifacts will obscure the true signal IF signatures in the TF domain and lead an inaccurate identification of the true IFs [11].

C. Sparse Reconstruction of Time-Frequency Representation

The Wigner-Ville Distribution (WVD) is often referred to as the prototype bilinear TF distribution. It can be obtained via the DFT of the IAF $R_{xx}(t,\tau)$ with respect to τ, i.e.,

$$W_{xx}(t,f) = \mathcal{F}_\tau[R_{xx}(t,\tau)] = \sum_\tau R_{xx}(t,\tau)e^{-\jmath 4\pi f\tau}, \tag{4}$$

where $\jmath = \sqrt{-1}$ is the imaginary unit. In (4), 4π is used instead of 2π since the time-lag τ is required to be an integer so that the actual lag in (2) is 2τ. The WVD can also be obtained from the 2-D DFT of the ambiguity function (AF),

$$G_{xx}(\theta,\tau) = \mathcal{F}_t\left[R_{xx}(t,\tau)\right] = \sum_t R_{xx}(t,\tau)e^{-\jmath 2\pi\theta t}, \tag{5}$$

which is the DFT of the IAF with respect to time t.

The bilinear nature of the WVD renders cross-terms to appear midway between true signal components in the case of nonlinear or multicomponent signals. Such cross-terms prohibit accurate analysis and interpretation of the signal IF signatures [16]. To remedy this issue, TF kernels are designed to suppress cross-terms while preserving auto-terms. TF kernels can be classified into data-independent (fixed) kernels and data-dependent (adaptive) kernels. Choi-Williams [17] and cone-kernel [18] are examples of fixed kernels, whereas the AOK is a commonly used adaptive kernel. Generally, adaptive kernels outperform fixed counterparts since they are optimized based on the signal characteristics.

Because FM signals are sparsely presented in the TF domain, obtaining TFR can be viewed as a sparse reconstruction problem [7], [11], [19]. Denote $\boldsymbol{y}^t$ as an IAF slice that contains all IAF entries along the τ dimension corresponding to time t, and $\boldsymbol{s}^t$ as the corresponding TFR slice for the same time t. Here, $\boldsymbol{y}^t$ may denote the original IAF, which corresponds to the WVD, or its smoothed version as a result of applying a TF kernel. The non-zero entries of $\boldsymbol{s}^t$ can be reconstructed as

$$\hat{\boldsymbol{s}}^t = \arg\min_{\boldsymbol{s}^t} \|\boldsymbol{s}^t\|_0 \quad \text{s.t.} \quad \boldsymbol{y}^t = \boldsymbol{\Phi}\boldsymbol{s}^t, \quad \forall t, \tag{6}$$

where $\boldsymbol{\Phi}$ is the IDFT dictionary matrix. Many compressive sensing techniques, such as the orthogonal matching pursuit (OMP) [20], least absolute shrinkage and selection operator (LASSO) [21], and Bayesian sparse learning techniques [22], [23], can be used to solve problem (6).

III. Proposed TFR Reconstruction Technique

In this section, we describe the proposed technique which improves the TFR reconstruction through three major stages.

A. Stage 1: IAF Interpolation via Atomic Norm

Assume that there are P frequency components at time instant t, i.e., the TF slice $\boldsymbol{w}^t$ is a sparse vector with P non-zero components. Because the IAF is the IDFT of WVD with respect to f, the IAF slice $\boldsymbol{y}^t \in \mathbb{C}^Q$ at time instant t can be expressed as

$$\boldsymbol{y}^t = \mathcal{F}_f^{-1}(\boldsymbol{w}^t) = \sum_{p=1}^{P} c_p e^{\jmath 2\pi f_p \boldsymbol{\tau}}, \tag{7}$$

where c_p denotes the complex amplitude of the p-th signal component, f_p is the corresponding signal frequency, and $\boldsymbol{\tau} = [\tau_1, \cdots, \tau_Q]^{\mathrm{T}}$ is the time lag vector. We solve this problem in the context of Hankel matrix completion [24] by forming the following Hankel matrix from $\boldsymbol{y}^t$:

$$\boldsymbol{H}^t = \mathcal{H}(\boldsymbol{y}^t, q_1) = \begin{bmatrix} y_1^t & y_2^t & \cdots & y_{q_2}^t \\ y_2^t & y_3^t & \cdots & y_{q_2+1}^t \\ \vdots & \vdots & \ddots & \vdots \\ y_{q_1}^t & y_{q_1+1}^t & \cdots & y_Q^t \end{bmatrix}, \tag{8}$$

where q_1 is the pencil parameter, which is usually set to $\lceil Q/2 \rceil$, and $q_2 = Q - q_1 + 1$.

All the columns in $\boldsymbol{H}^t$ share the same P frequency components. An atom to represent $\boldsymbol{H}^t$ can be expressed as

$$\boldsymbol{A}(f,\boldsymbol{\phi}) = \boldsymbol{a}(f)\boldsymbol{\phi}^{\mathrm{H}}, \tag{9}$$

where $\boldsymbol{a}(f) = e^{\jmath 2\pi f\boldsymbol{\tau}} \in \mathbb{C}^{q_1}$, $f \in [0,1)$, $\boldsymbol{\phi} \in \mathbb{C}^{q_2}$ with $\|\boldsymbol{\phi}\|_2 = 1$. The frequency set is continuously defined and not restricted on the grid. Then, we can define the atom set for $\boldsymbol{H}^t$ as $\mathcal{A} = \{\boldsymbol{A}(f,\boldsymbol{\phi}) | f \in [0,1), \|\boldsymbol{\phi}\|_2 = 1\}$. Following the recipe in [25]–[27], atomic norm of $\boldsymbol{H}^t$ can be expressed as

$$\begin{aligned} \|\boldsymbol{H}^t\|_{\mathcal{A}} &= \inf\left\{\beta > 0 : \boldsymbol{H}^t \in \beta\mathrm{conv}(\mathcal{A})\right\} \\ &= \inf\left\{\sum_p |c_p| : \boldsymbol{H}^t = \sum_p |c_p|\boldsymbol{a}(f_p,\boldsymbol{\phi}_p)\right\}, \end{aligned} \tag{10}$$

where $\mathrm{conv}(\mathcal{A})$ is the convex hull of $\mathcal{A}$. Then, the signal recovery from a noisy measurement can be converted into an atomic norm minimization problem as

$$\hat{\boldsymbol{y}}^t = \arg\min_{\boldsymbol{y}^t} \|\mathcal{H}(\boldsymbol{y}^t, q_1)\|_{\mathcal{A}} \quad \text{s.t.} \quad \|\boldsymbol{y}_{\Omega^t}^t - \boldsymbol{z}_{\Omega^t}^t\|_2 \le \epsilon, \tag{11}$$

where $\boldsymbol{z}^t = [R_{rr}(t,\tau_1), \cdots, R_{rr}(t,\tau_Q)]^{\mathrm{T}}$ denotes the t-th slice of the IAF of the observed signal $r(t)$, and $\Omega^t = [R_{RR}(t,\tau_1), \cdots, R_{RR}(t,\tau_Q)]^{\mathrm{T}}$ denotes the observation pattern, i.e., the t-th slice of the IAF of the observation mask $R(t)$, and ϵ denotes the noise. $\|\mathcal{H}(\boldsymbol{y}^t, q_1)\|_{\mathcal{A}}$ in (11) can be computed via semidefinite programming (SDP) [26], [28] as:

$$\begin{aligned} &\min_{\boldsymbol{u},\boldsymbol{W},\boldsymbol{y}^t} \ \mathrm{Tr}(\mathcal{T}(\boldsymbol{u})) + \mathrm{Tr}(\boldsymbol{W}) \\ &\text{s.t.} \quad \begin{bmatrix} \mathcal{T}(\boldsymbol{u}) & \mathcal{H}(\boldsymbol{y}^t, q_1) \\ \mathcal{H}(\boldsymbol{y}^t, q_1)^{\mathrm{H}} & \boldsymbol{W} \end{bmatrix} \succeq 0, \|\boldsymbol{y}_{\Omega^t}^t - \boldsymbol{z}_{\Omega^t}^t\|_2 \le \epsilon. \end{aligned} \tag{12}$$

The structure of the IAF can be used to reduce the dimension of unknowns and renders better TFR reconstruction performance. It is clear from (2) that $\boldsymbol{y}^t$ is Hermitian symmetrical about $\tau_I = 0$, where I is the index of the center element in $\boldsymbol{\tau}$, i.e., $\left[y^t_{I-1}, \cdots, y^t_2, y^t_1\right]^{\mathrm{H}} = \left[y^t_{I+1}, \cdots, y^t_{Q-1}, y^t_Q\right]^{\mathrm{T}}$. Then,

$$\boldsymbol{y}^t = \left[y^t_1, \cdots, y^t_{I-1}, y^t_I, \left(y^t_{I-1}\right)^*, \cdots, \left(y^t_1\right)^*\right]^{\mathrm{T}}. \tag{13}$$

As such, the number of unknowns in $\boldsymbol{y}^t$ is reduced to half.

When dealing with a finite data sequence, the IAF has a diamond shape with a time-varying width of $Q = T - |T+1-2t|$ because of zero-padding. When Q is small, the recovery of missing entries of $\boldsymbol{y}^t$ becomes unreliable. To avoid this issue, we recover the missing entries of $\boldsymbol{y}^t$ based on the approach described above only for $0.25T \le t \le 0.75T$. For the missing entries in the triangular regions of $t < 0.25T$ and $t > 0.75T$ (see Fig. 1), we utilize the sparsity of the short-time AF and the similar DFT relationship between the IAF and the AF to recover the missing entries for $0 \le \tau \le 0.25T$, whereas those for $-0.25T \le \tau < 0$ are obtained based on the conjugate property of the IAF. The obtained IAF after performing the atomic norm interpolation is denoted as $\hat{R}^{(1)}_{rr}(t,\tau)$.

B. Stages 2 and 3: TF Kernel and Rank Reduction

Because the use of atomic norm cannot suppress cross-terms which exist even in the absence of missing samples, we use the AOK to obtain a signal-adaptive kernel, denoted in the AF domain as $\Psi(t,\tau)$, and obtain the kerneled IAF as,

$$\hat{R}^{(2)}_{rr}(t,\tau) = \mathcal{F}^{-1}_t\left[\hat{R}^{(1)}_{rr}(t,\tau)\Psi(t,\tau)\right]. \tag{14}$$

After the previous two stage processing, true signal components would dominate the interpolated and kerneled IAF. Next, we utilize the low-rank property of the true IAF to further reduce the residual effects of cross-terms and artifacts in $\hat{R}^{(2)}_{rr}(t,\tau)$. Denote $\ddot{\boldsymbol{y}}^t$ as the t-th column of IAF $\hat{R}^{(2)}_{rr}(t,\tau)$. For each time instant t for $t = 1, \cdots, T$, convert $\ddot{\boldsymbol{y}}^t$ to a Hankel matrix $\ddot{\boldsymbol{H}}^t \in \mathbb{C}^{q_1 \times q_2}$ in the same way as (8). The singular value decomposition (SVD) yields:

$$\ddot{\boldsymbol{H}}^t = \boldsymbol{U}^t \boldsymbol{\Sigma}^t \left(\boldsymbol{V}^t\right)^{\mathrm{H}}, \tag{15}$$

where $\boldsymbol{U}^t \in \mathbb{C}^{q_1 \times q_1}$ and $\boldsymbol{V}^t \in \mathbb{C}^{q_2 \times q_2}$ are column-orthonormal matrices, and $\boldsymbol{\Sigma}^t \in \mathbb{C}^{q_1 \times q_2}$ is a diagonal matrix with singular values $[\sigma^2_1, \sigma^2_2, \cdots, \sigma^2_{\min(q_1,q_2)}]$ located in the diagonal. We select N principal singular values and form $\mathrm{diag}(\bar{\boldsymbol{\Sigma}}^t) = [\sigma^2_1, \cdots, \sigma^2_N, \cdots, 0, 0]$ with $0 < N \le \min(q_1, q_2)$. A rule of thumb for determining the value of N is to retain enough singular values to make up around 95% of the energy in $\boldsymbol{\Sigma}^t$ [29]. Thus, the t-th column of the rank-reduced kerneled interpolated IAF $\hat{R}^{(3)}_{rr}(t,\tau)$ is obtained as

$$\left[\hat{R}^{(3)}_{rr}(t,\tau_1), \cdots, \hat{R}^{(3)}_{rr}(t,\tau_Q)\right]^{\mathrm{T}} = \bar{\boldsymbol{y}}^t, \tag{16}$$

where $\bar{\boldsymbol{y}}^t = \hbar\left[\boldsymbol{U}^t \bar{\boldsymbol{\Sigma}}^t \left(\boldsymbol{V}^t\right)^{\mathrm{H}}\right]$. $\hat{R}^{(3)}_{rr}(t,\tau)$ is used to reconstruct the TFR using OMP by solving (6) for each time instant.

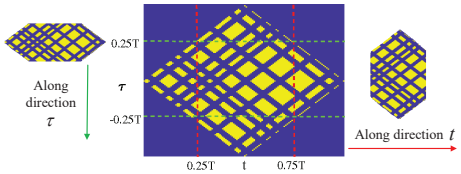

Fig. 1. IAF with burst missing samples for atomic norm-based processing.

IV. Simulation Results

We consider two sets of FM signals, i.e., two-component linear and nonlinear FM signals with different amplitudes,

$$x(t) = \exp\left(j2\pi\Phi_1(t)\right) + 0.5\exp\left(j2\pi\Phi_2(t)\right), \tag{17}$$

$t = 1, \cdots, T$. We assume $T = 128$, and each missing burst contains 4 missing entries. Unless otherwise specified, there are 48 missing samples and no noise is considered.

A. Two-component Linear FM

We first consider the following two-component linear FM signal with their phase laws given as:

$$\Phi_1(t) = 0.05t + 0.2t^2/T, \ \Phi_2(t) = 0.2t^2/T. \tag{18}$$

Figs. 2(a) and 2(b) show the IAF and the WVD in the absence of missing samples. The missing entries in the IAF are clearly seen in Fig. 2(c) and cause localized artifacts in the WVD as shown in Fig. 2(d). Note that the amplitude difference makes the detection of the weak signal challenging. Fig. 2(e) shows that the combined use of the AOK and the OMP fails to effectively mitigate the artifacts and detect the weak signal.

Fig. 2(f) depicts the recovered IAF $\hat{R}^{(1)}_{rr}(t,\tau)$ via the atomic norm-based reconstruction (Stage 1), which restores the missing entries, and the result is very close to the ideal IAF $R_{xx}(t,\tau)$ shown in Fig. 2(a) obtained in the absence of missing samples. The corresponding WVD is shown in Fig. 2(g), which is close to the ideal WVD, shown in Fig. 2(b), obtained in the absence of missing samples.

Figs. 2(h) and 2(i) show the IAF $\hat{R}^{(2)}_{rr}(t,\tau)$ and the corresponding TFR after further applying the AOK (Stage 2). It is clear that both artifacts and cross-terms are substantially mitigated but there are still some residual artifacts. Figs. 2(j) and 2(k) show the IAF and clear two-component TFR after reduced-rank processing (Stage 3). Fig. 2(l) shows the final TFR obtained through sparse reconstruction using OMP. Compared to Fig. 2(d), the occupancy rate of the auto-terms of the TFR in Fig. 2(l) increases from 39.7% to 98.5%.

B. Two-component nonlinear FM

Now we consider a two-component nonlinear FM signal with the following instantaneous phase laws:

$$\begin{aligned}\Phi_1(t) &= 0.05t + 0.05t^2/T + 0.1t^3/T^2,\\ \Phi_2(t) &= 0.15t + 0.025t^2/T + 0.1t^3/T^2.\end{aligned} \tag{19}$$

Fig. 3(a) shows the IAF in the absence of missing samples, and Fig. 3(b) shows the corresponding WVD.

In the sequel, we consider the signal in the presence of burst missing samples. Fig. 3(c) shows the IAF which exhibits clear missing entry patterns. Fig. 3(d) shows the corresponding WVD with artifacts around the signal IFs. The TFR obtained from sparse reconstruction using AOK and OMP, as shown in

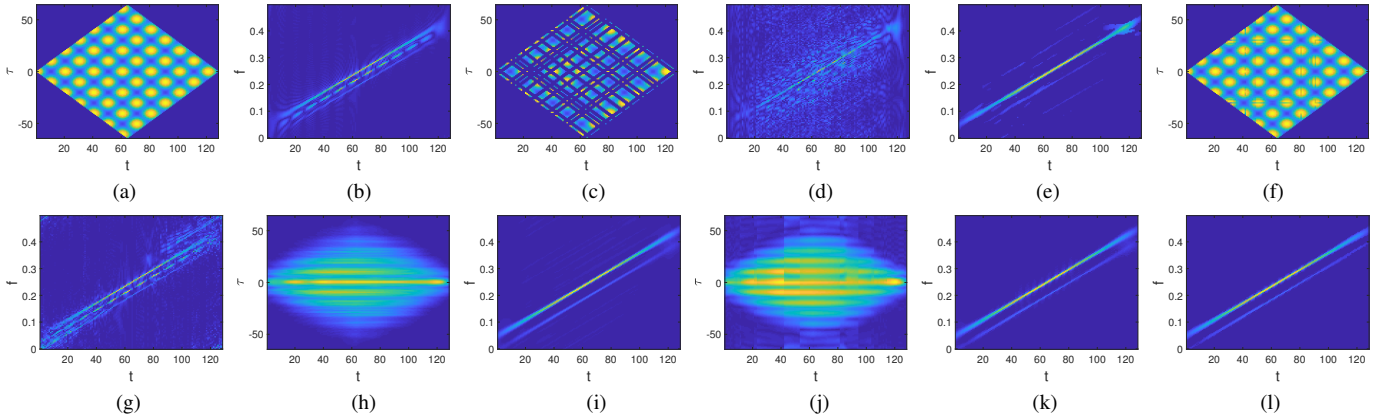

Fig. 2. Results for two-component linear FM signal. (a) IAF without burst missing samples; (b) WVD without burst missing samples; (c) IAF with burst missing samples; (d) WVD with burst missing samples; (e) TFR using OMP and AOK with burst missing samples; (f) IAF for stage 1 (atomic norm); (g) WVD for stage 1 (atomic norm); (h) IAF for stage 2 (atomic norm + AOK); (i) TFR for stage 2 (atomic norm + AOK); (j) IAF for stage 3 (atomic norm + AOK + rank deduction); (k) TFR for stage 3 (atomic norm + AOK + rank deduction); (l) proposed TFR.

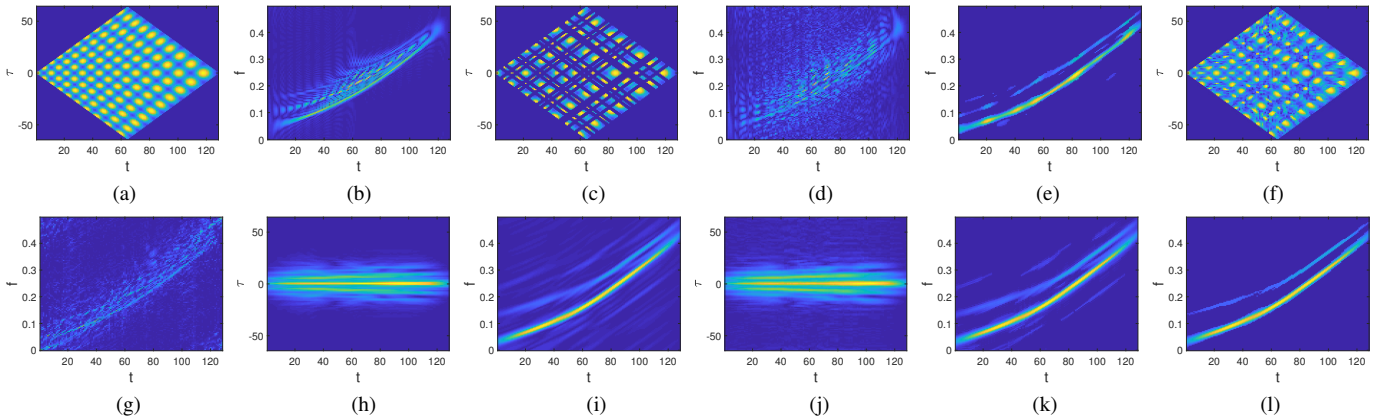

Fig. 3. Results for two-component nonlinear FM signal. (a) IAF without burst missing samples; (b) WVD without burst missing samples; (c) IAF with burst missing samples; (d) WVD with burst missing samples; (e) TFR using OMP and AOK with burst missing samples; (f) IAF for stage 1 (atomic norm); (g) WVD for stage 1 (atomic norm); (h) IAF for stage 2 (atomic norm + AOK); (i) TFR for stage 2 (atomic norm + AOK); (j) IAF for stage 3 (atomic norm + AOK + rank deduction); (k) TFR for stage 3 (atomic norm + AOK + rank deduction); (l) proposed TFR.

Fig. 3(e), provides a much better result but fails to consistently identify the IFs of the two components, as the second signal component is misguided by the cross-terms at the beginning of time. Fig. 3(f) depicts the IAF $\hat{R}^{(1)}_{rr}(t,\tau)$ after atomic norm-based recovery where most missing entries are correctly interpolated. The resulting WVD shown in Fig. 3(g) is much closer to the WVD in the full-data case as shown in Fig. 3(b), and exhibits a significant improvement from Fig. 3(d). Clearly, the nonlinear FM signal case is much more challenging as compared to the linear FM signal counterpart because of the much more complicated TF cross-terms involved in this case.

As depicted in Figs. 3(h) and 3(i), the use of AOK further substantially mitigates the cross-terms, yielding much cleaner TFR. The subsequent rank reduction reduces residual aliasing and renders much more consistent TFR, as shown in Figs. 3(j) and 3(k). Finally, applying the OMP yields high-resolution TFR results with a high fidelity, as shown in Fig. 3(l). Compared to Fig. 3(d), the occupancy rate of the auto-terms of the TFR in Fig. 3(l) increases from 14.06% to 98.11%.

Next, we consider noisy signal measurements with different levels of the input SNR and missing rate. We report the mean square error (MSE) between the interpolated IAF and the ideal IAF (obtained from noiseless signal with no missing samples) as a performance indicator in Table I. The baseline used for comparison is the original IAF obtained without performing interpolation. 50 simulation runs are performed for each scenario. As shown in Table I, our proposed method consistently reduces the MSE of the reconstructed IAF.

TABLE I
MSE BETWEEN STAGE 1 IAF (Stg1) AND ORIGINAL IAF (Org)

SNR (dB)	Linear FM				Nonlinear FM			
	37.5%		50%		37.5%		50%	
	Stg1	Org	Stg1	Org	Stg1	Org	Stg1	Org
Inf	0.00	0.57	0.14	0.63	0.22	0.44	0.45	0.60
25	0.02	0.57	0.17	0.64	0.23	0.45	0.45	0.60
15	0.06	0.58	0.24	0.64	0.27	0.47	0.48	0.60
5	0.35	0.69	0.49	0.71	0.52	0.58	0.65	0.67

V. CONCLUSION

In this letter, we propose a new algorithm to achieve high-fidelity TFR reconstruction for multi-component FM signals in the presence of burst missing samples. The proposed algorithm effectively mitigates the effect of burst missing samples by interpolating the missing entries in the IAF domain via the atomic norm-based approach. The AOK is then used to suppress the cross-terms, and rank deduction technique further reduces the residual aliasing. The effectiveness of the proposed algorithm is verified for both linear and nonlinear FM signals.

REFERENCES

[1] A. Papandreou-Suppappola (Editor), *Applications in Time-Frequency Signal Processing*, CRC Press, 2002.

[2] S. Liu, Y. D. Zhang, and T. Shan, "Detection of weak astronomical signals with frequency-hopping interference suppression," *Digital Signal Process.*, vol. 72, pp. 1–8, Jan. 2018.

[3] S. Liu, Y. D. Zhang, T. Shan and R. Tao, "Structure-aware Bayesian compressive sensing for frequency-hopping spectrum estimation with missing observations," *IEEE Trans. Signal Process.*, vol. 66, no. 8, pp. 2153–2166, April 2018.

[4] Y. Chen, D. Joffre, and P. Avitabile, "Underwater dynamic response at limited points expanded to full-field strain response," *ASME J. Vib. Acoust.*, vol. 140, no. 5, pp. 051016-1–051016-9, Oct. 2018.

[5] Y. Chen, P. Logan, P. Avitabile, and J. Dodson, "Non-model based expansion from limited points to an augmented set of points using Chebyshev polynomials," *Exp. Tech*, pp. 1–23, 2019.

[6] S. Zhang, Y. Gu, and Y. D. Zhang, "Robust Astronomical Imaging in the Presence of Radio Frequency Interference," *J. Astronom. Instrument.*, vol. 8, no. 1, pp. 1940012-1–1940012-15, 2019.

[7] Y. D. Zhang, M. G. Amin, and B. Himed, "Reduced interference time-frequency representations and sparse reconstruction of undersampled data," in *Proc. European Signal Process. Conf.*, Marrakech, Morocco, Sept. 2013, pp. 1–5.

[8] M. G. Amin, B. Jakonovic, Y. D. Zhang, and F. Ahmad, "A sparsity-perspective to quadratic time-frequency distributions," *Digital Signal Process.*, vol. 46, pp. 175–190, Nov. 2015.

[9] Y. D. Zhang, "Resilient quadratic time-frequency distribution for FM signals with gapped missing data," in *Proc. IEEE Radar Conf.*, Seattle, WA, May 2017, pp. 1765–1769.

[10] V. S. Amin, Y. D. Zhang, and B. Himed, "Improved instantaneous frequency estimation of multi-component FM signals," in *Proc. IEEE Radar Conf.*, Boston, MA, April 2019.

[11] V. S. Amin, Y. D. Zhang, and B. Himed, "Sparsity-based time-frequency representation of FM signals with burst missing samples," *Signal Process.*, vol. 155, pp. 25–43, Feb. 2019.

[12] P. Stoica, J. Li, and J. Ling, "Missing data recovery via a non-parametric iterative adaptive approach," *IEEE Signal Process. Lett.*, vol. 16, no. 4, pp. 241–244, April 2009.

[13] A. Moghtaderi, P. Borgnat, and P. Flandrin, "Gap-filling by the empirical mode decomposition," in *Proc. IEEE Int. Conf. Acoust. Speech Signal Process. (ICASSP)*, Kyoto, Japan, March 2012, pp. 3821–3824.

[14] B. Jokanovic and M. Amin, "Reduced interference sparse time-frequency distributions for compressed observations," *IEEE Trans. Signal Process.*, vol. 63, no. 24, pp. 6698-6709, Dec. 2015.

[15] D. L. Jones and R. G. Baraniuk, "An adaptive optimal kernel time-frequency representation," *IEEE Trans. Signal Process.*, vol. 43, no. 10, pp. 2361–2371, Oct. 1995.

[16] B. Boashash (ed.), *Time-Frequency Signal Analysis and Processing: A Comprehensive Reference, 2nd ed.* Academic Press, 2015.

[17] H. I. Choi and W. J. Williams, "Improved time-frequency representation of multicomponent signals using exponential kernels," *IEEE Trans. Acoust., Speech, Signal Process.*, vol. 37, no. 6, pp. 862–871, June 1989.

[18] Y. Zhao, L. E. Atlas, and R. J. Marks, "The use of cone-shaped kernels for generalized time-frequency representations of nonstationary signals," *IEEE Trans. Acoust., Speech, Signal Process.*, vol. 38, no. 7, pp. 1084–1091, July 1990.

[19] P. Flandrin and P. Borgnat, "Time-frequency energy distributions meet compressed sensing," *IEEE Trans. Signal Process.*, vol. 58, no. 6, pp. 2974-2982, June 2010.

[20] J. A. Tropp and A. C. Gilbert, "Signal recovery from random measurements via orthogonal matching pursuit," *IEEE Trans. Inf. Theory*, vol. 53, no. 12, pp. 4655–4666, Dec. 2007.

[21] R. J. Tibshirani, "Regression shrinkage and selection via the LASSO," *J. Royal Statistical Society*, no. 1, vol. 58, pp. 267–288, 1996.

[22] S. Ji, Y. Xue, and L. Carin, "Bayesian compressive sensing," *IEEE Trans. Signal Process.*, vol. 56, no. 6, pp. 2346–2356, June 2008.

[23] Q. Wu, Y. D. Zhang, M. G. Amin, and B. Himed, "Complex multitask Bayesian compressive sensing," in *Proc. IEEE Int. Conf. Acoust. Speech Signal Process. (ICASSP)*, Florence, Italy, May 2014.

[24] Y. Chen and Y. Chi, "Harnessing structures in big data via guaranteed low-rank matrix estimation," July 2018. Available at https://arxiv.org/abs/1802.08397

[25] V. Chandrasekaran, B. Recht, P. A. Parrilo, and A. S. Willsky, "The convex geometry of linear inverse problems," *Found. Comput. Math.*, vol. 12, no. 6, pp. 805–849, Dec. 2012.

[26] G. Tang, B. Bhaskar, P. Shah, and B. Recht, "Compressed sensing off the grid," *IEEE Trans. Inf. Theory*, vol. 59, no. 11, pp. 7465–7490, Nov. 2013.

[27] Z. Yang and L. Xie, "On gridless sparse methods for line spectral estimation from complete and incomplete data," *IEEE Trans. Signal Process.*, vol. 63, no. 12, pp. 3139–3153, June 2015.

[28] Y. Li and Y. Chi, "Off-the-grid line spectrum denoising and estimation with multiple measurement vectors," *IEEE Trans. Signal Process.*, vol. 64, no. 5, pp. 1257–1269, March 2016.

[29] S. Zhang, Y. Gu, C. -H. Won, and Y. D. Zhang, "Dimension-reduced radio astronomical imaging based on sparse reconstruction," in *Proc. IEEE Sens. Array Multichannel Signal Process. Workshop*, Sheffield, UK, July 2018.